IEEE Open Journal of Antennas and Propagation

Received XX Month, XXXX; revised XX Month, XXXX; accepted XX Month, XXXX; Date of publication XX Month, XXXX; date of current version XX Month, XXXX.

*Digital Object Identifier 10.1109/OJAP.2020.1234567*

# A Miniaturized Quad-Port Circularly Polarized MIMO Antenna for mmWave Wireless Applications

**ABDUL MAJEED*, YEJUN HE*, (Senior Member, IEEE), AND YI HUANG†, (Fellow, IEEE)**

[1]State Key Laboratory of Radio Frequency Heterogeneous Integration, Sino-British Antennas and Propagation Joint Laboratory of MOST, Guangdong Engineering Research Center of Base Station Antennas and Propagation, Shenzhen Key Laboratory of Antennas and Propagation, College of Electronics and Information Engineering, Shenzhen University, Shenzhen 518060, China.
[2]Department of Electrical Engineering and Electronics, the University of Liverpool, UK.

CORRESPONDING AUTHOR: YEJUN HE (e-mail: heyejun@126.com)

This work was supported in part by the National Key Research and Development Program of China under Grant 2023YFE0107900; in part by National Natural Science Foundation of China under Grants 62171289 and 62071306, and in part by the Shenzhen Science and Technology Program under grant JCYJ20241202124219023.

**ABSTRACT** This paper presents a miniaturized quad-port circularly polarized (CP) multiple-input multiple-output (MIMO) slot antenna with enhanced isolation, gain, and diversity performance for millimeter-wave (mmWave) applications. Each port excites an identical notched rectangular slot via a 50 Ω microstrip line. A simple "+"-shaped slot etched on the ground plane improves inter-element isolation. Additionally, a split ring resonator (SRR)-based reflector, designed at the antenna's fundamental mode and placed above the array, improves the gain by 1 dBic and further reduces mutual coupling within a compact size of $14\times14\times0.508$ mm$^3$ ($1.31\lambda_0\times1.31\lambda_0\times0.047\lambda_0$), where $\lambda_0$ is free space wavelength at the operating frequency of 28 GHz. The proposed CP MIMO antenna has an impedance bandwidth (IBW) of 25.80–28.96 GHz, an axial ratio bandwidth (ARBW) of 26.56–28.96 GHz, a gain of 6.0 dBic, isolation of $\leq -22$ dB, and a radiation efficiency exceeding 94%. Excellent diversity performance is demonstrated through a low envelope correlation coefficient (ECC), high diversity gain (DG), a mean effective gain (MEG), and low channel capacity loss (CCL). An equivalent circuit model of the MIMO antenna is analyzed. Measured and simulated results show strong agreement, confirming the antenna's suitability for mmWave wireless communications and smart devices.

**INDEX TERMS** Axial ratio, circular polarization, mmWave, 5G network, MIMO antenna.

## I. INTRODUCTION

THE research community is focusing on the rapid advancements in wireless communication technologies. The number of users is increasing rapidly, along with the demand for high data rates [1]. Multiple-input-multiple-output technology improves data rates, reliability, and channel capacity in multipath fading environments without requiring additional transmission power or bandwidth. MIMO systems enhance the communication performance by using multiple antenna elements at both the transmitter and receiver. Various MIMO antennas have been developed specifically for 5G applications in mmWave frequency bands [2]. MIMO antennas typically exhibit linear polarization (LP), which creates a multipath fading problem. Linear polarization limits the channel capacity of the multiple-input multiple-output antenna. To overcome this challenge, circularly polarized antennas have recently gained considerable attention in MIMO system design [3], [4]. Regardless of orientation independence, the circularly polarized antennas are preferred over LP antennas in terms of wireless connectivity due to their reliable connection between the sending and receiving device. In dynamic situations, the circularly polarized antennas, particularly left-handed circularly polarized (LHCP) and right-handed circularly polarized (RHCP), significantly reduce multipath interference, improve signal stability and MIMO system channel capacity [5], [6]. In MIMO antenna systems, isolation between closely spaced radiating elements is a critical design parameter that directly affects overall system performance. Poor isolation leads to mutual coupling, which causes signal distortion, impedance mismatch, and degra-

dation of diversity characteristics, thereby reducing channel capacity and radiation efficiency. At mmWave frequency bands, achieving high isolation is particularly challenging due to short wavelengths and dense integration, which increase electromagnetic coupling between elements. Therefore, highly isolated and circularly polarized MIMO antennas within the limited space of modern wireless devices present a considerable challenge [7], [8]. Circular polarization in single microstrip patch element is obtained by generating two resonant orthogonal modes characterized by identical amplitudes with a phase difference of 90° [9]. Typically, circular polarization is achieved by adding a geometric structure called a stub to the patch's edge [10]. Moreover, CP can be achieved by incorporating slots into the radiating patch [11], cutting off the corners of a rectangular microstrip patch element, or truncating the corners [12]. The single patch CP antenna can be modified by incorporating a multi-element MIMO configuration to enhance its spatial diversity and link reliability [13]. Integrating circular polarization improves the performance in mobile and adverse weather conditions [14], [15]. In addition to ensuring polarization diversity, the MIMO systems should have multiple antenna elements closely spaced to maximize the compactness. However, MIMO performance gains scale with the number of antennas, presenting design challenges. Densely packed antenna arrays can lead to strong mutual coupling, potentially degrading channel capacity and diversity performance [16].

Several antenna designs have been proposed to reduce mutual coupling in MIMO systems, including 6-shaped and hexagonal nested neutralization line (HN-NL) [17], tapered slot antennas [18], [19], meander line antenna [20], slotted rectangular patches [21], and parasitic structures [22]–[24]. Additionally, MIMO antenna isolation can be enhanced using physically separated ground planes [25] and spatial diversity techniques [26]. Moreover, the split-ring resonators [27] and electromagnetic bandgap (EBG) [28] materials have been used to enhance the performance and isolation of MIMO systems. Recent research has introduced several innovative solutions, including a mmWave MIMO magnetoelectric (ME) dipole antenna array [29] and a four-port orthogonal circularly polarized MIMO antenna equipped with a polarization converter [30]. Additionally, a flexible MIMO antenna featuring E-shaped and rectangular slots has been proposed to improve isolation in the 26/31 GHz 5G bands [31]. Furthermore, a compact double-sided frequency selective surface (FSS) absorbing wall for decoupling 5G antenna arrays has demonstrated the ability to achieve over 20 dB of isolation [32]. Despite these advancements, several challenges remain, such as narrow bandwidth [19], [21], [26], [30], [32], inadequate isolation [19], [25], [28], [29], [32], large physical dimensions [9], [19], [21], [27], [32], and low gain performance [21], [22], [24], [27], [30], [32].

This paper presents a quad-port circularly polarized MIMO slot antenna with enhanced isolation, using a simple "+"-shaped slot configuration, with following contributions.

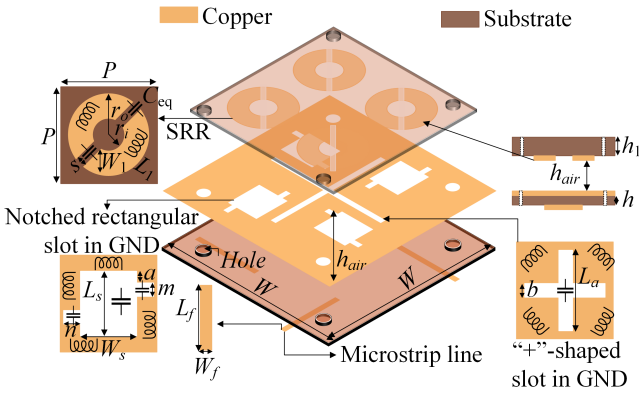


**FIGURE 1. Deployed view of the proposed MIMO antenna with SRR superstrate.**

- A "+"-shaped slot in the ground reduces the mutual coupling, and CP radiation minimizes polarization mismatch in 5G mmWave.
- An SRR-based reflector improves gain by 1 dBi, further reduces mutual coupling, and achieves high-efficiency suitable for low-power 5G devices (smartphones/IoT).
- The MIMO diversity performance, characterized by low ECC, high DG, favorable MEG, and low CCL, ensures robust signal quality in multipath mmWave applications.

The upcoming section of this paper includes the antenna design methodology of the proposed antenna in Section II, the SRR-reflector-based proposed MIMO antenna in Section III, an equivalent circuit model in Section IV, experimental results and discussion in Section V, an analysis of diversity performances in Section VI, and a comparison in Section VII. Finally, Section VIII concludes the paper.

## II. Antenna design Methodology

### A. Antenna Configuration

Fig. 1 illustrates the perspective view of the proposed MIMO antenna incorporating an SRR-based reflector superstrate. The overall MIMO antenna dimensions are $20\times20\times0.813$ mm$^3$ ($1.87\lambda_0\times1.87\lambda_0\times0.076\lambda_0$). A 50 Ω microstrip feed line is implemented on Rogers RO4003C substrate with a dielectric constant of 3.55 and a thickness of 0.305 mm. On the backside of the substrate, a rectangular notch and a "+"-shaped slot are etched on the ground plane to excite circular polarization. A $2\times2$ array of SRR reflectors, measuring $14\times14$ mm$^2$, is printed on a Rogers RT5880 substrate with a height of 0.508 mm ($h_1$) and placed above the antenna, with an air gap of 4.2 mm ($h_{air}$). Table 1 presents the optimized geometric parameters of the antenna, which are computed using the familiar transmission line theory of rectangular patch antenna [33].

### B. Design Equations for Single-Element Antenna

The proposed quad-port MIMO antenna consists of four radiators with simple microstrip feed lines, modeled using

**TABLE 1. Dimensions of the proposed MIMO antenna**

| Parameter | Value (mm) | Parameter | Value (mm) | Parameter | Value (mm) |
|---|---|---|---|---|---|
| $W$ | 20 | $b$ | 0.50 | $L_f$ | 8.0 |
| $W_f$ | 0.4 | $W_s$ | 3.0 | $m$ | 0.45 |
| $n$ | 0.2 | $L_s$ | 2.6 | $a$ | 0.20 |
| $L_a$ | 11.5 | $h_1$ | 0.508 | $P$ | 6.0 |
| $s$ | 0.2 | $r_o$ | 1.8 | $r_i$ | 0.63 |

analytical formulas. The dimensions of a single-element for a rectangular microstrip patch antenna are determined using fundamental equations. The resonance frequency can be calculated as follows [34]:

$$f_r = \frac{c}{2W\sqrt{\frac{(\varepsilon_r+1)}{2}}} \tag{1}$$

where $\varepsilon_r$ represents the substrate's relative permittivity and $c$ denotes the speed of light in meters per second (m/s). Based on the fundamental equation, the basic dimensions of the patch antenna are computed as follows [34]

$$W = \frac{c}{2f_r\sqrt{\frac{\varepsilon_r+1}{2}}} \tag{2}$$

$$L = \frac{c}{2f_r\sqrt{\varepsilon}_{eff}} - 0.824h\left(\frac{(\varepsilon_{eff}+0.3)\left(\frac{W}{h}+0.264\right)}{(\varepsilon_{eff}-0.258)\left(\frac{W}{h}+0.8\right)}\right) \tag{3}$$

The effective length $L_{(eff)}$ of the patch is determined by using (4).

$$L\,(eff) = \frac{c}{2f_o\sqrt{\varepsilon}_{(eff)}} \tag{4}$$

where $\varepsilon_{(eff)}$ is the effective permittivity and $h$ is the height of substrate. The length and width of the ground can be calculated as follows

$$L_g = 6h + L \tag{5}$$

$$W_g = 6h + W \tag{6}$$

The proposed quad-port MIMO antenna system is excited by a 50 Ω feed line with a width of 0.4 mm. For multiple antenna elements, the desired impedance matching is determined as follows:

$$W_{Z_0} = \left(\frac{377}{Z_0\sqrt{\varepsilon_r}} - 2\right) * h_s \tag{7}$$

where $Z_0$ represents the characteristics impedance of the feed line, $h_s$ denotes the height of the substrate, $W_{Z_0}$ indicates the width of a feed line for a specific impedance, and $\varepsilon_r$ is the permittivity of the dielectric material. The width of feedlines is set to obtain 50, 70.7 and 100 Ω according to (7).

### C. Design Equations for Split-Ring Resonator

The simple microstrip line antenna is transformed into a quad-port MIMO antenna system using a split-ring resonator placed above the antenna array. The SRR is a crucial component of the MIMO antenna system, which operates as a reflector. Since the unit cell of SRR operates as an LC circuit, we can determine the resonant frequency as follows [35]:

$$f_o = \frac{1}{2\pi\sqrt{LC}} \tag{8}$$

where $C$ represents the equivalent capacitance and $L$ denotes the effective inductance of the ring.

$$L = \frac{4.86\mu_0}{2}\,(r_0 - W1 - g)\left[ln\left(\frac{0.98}{\rho}\right) + 1.84\rho\right] \tag{9}$$

where $\rho$ is the filling factor of the inductance and is calculated by

$$\rho = \frac{W1+g}{r_0 - W1 - g} \tag{10}$$

The effective capacitance is determined by

$$C = \left(r_0 - \frac{3}{2}\,(W1+g)\,C_{pul}\right) \tag{11}$$

where $C_{pul}$ is the per unit length capacitance, which is calculated as

$$C_{pul} = \varepsilon_0\varepsilon_{eff}\frac{K\left(\sqrt{1-k^2}\right)}{K(k)} \tag{12}$$

where $\varepsilon_{eff}$ is the effective dielectric constant which can be stated as

$$\varepsilon_{eff} = \frac{\varepsilon_r+1}{2} \tag{13}$$

The function K($k$) represents the complete elliptical integral of the first kind, where $k$ is defined as follows:

$$k = \frac{g}{g+2W1} \tag{14}$$

The lumped model equivalent circuit of the SRR is designed using the given expressions, as illustrated in Fig. 1.

### D. Design Evaluation Process

Fig. 2 depicts the three-dimensional structure of the slot antenna from the top and back views. The stepwise design starts with a rectangular slot fed by a 50 Ω microstrip line (introduced in Step-I), followed by the Step-II ("+"-shaped) slot, the Step-III (rectangular slot), and the proposed notched rectangular slot configuration, with overall dimensions of $10\times10\times0.305$ mm$^3$. Fig. 3 shows the simulated results for each design iteration, including impedance bandwidth, axial ratio, and gain, obtained using CST Microwave Studio 2022. In the initial three configurations (Step-I, Step-II, Step-III), the antenna achieves impedance matching ($|S_{11}| \leq -10$ dB) at resonant frequencies of 24 GHz, 25.9 GHz, and 28.3 GHz, corresponding to 10 dB IBW ranges of 24–25 GHz, 25.8–26.2 GHz, and 27.8–28.5 GHz, respectively. However, an axial ratio of 40 dB indicates linear polarization performance, with a gain of approximately 5.0 dBi and 6.0 dBi for the latter designs. By introducing a small rectangular notch into

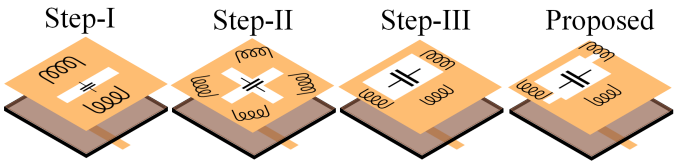


**FIGURE 2.** 3D configuration stepwise slot antenna design.

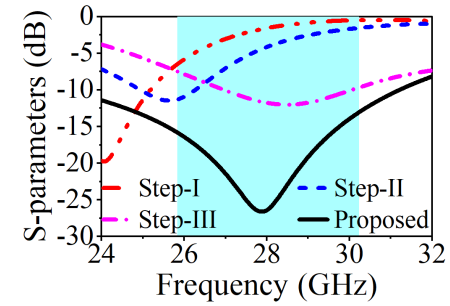


(a)

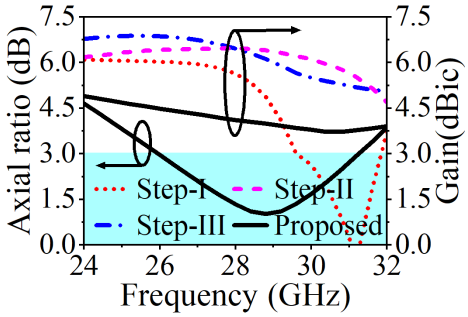


(b)

**FIGURE 3.** The simulated results of stepwise antenna design. (a) S-parameters in dB. (b) Axial ratio with a peak gain (dBic).

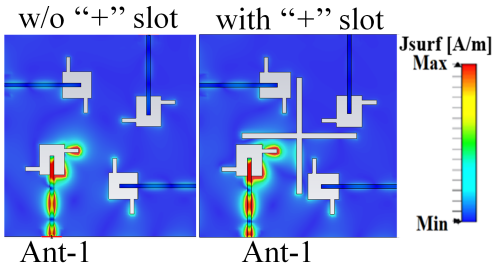


(a)

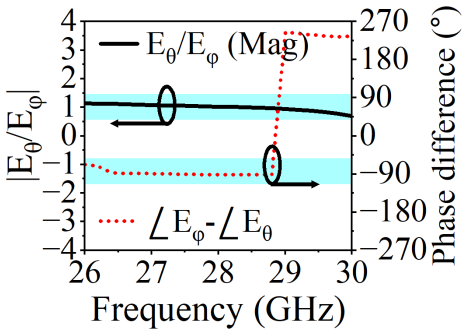


(b)

**FIGURE 4.** (a) Surface current distribution of Ant-1 w/o and with"+"-shaped slot. (b) $|E_\theta/E_\varphi|$ (Mag) with phase difference (°).

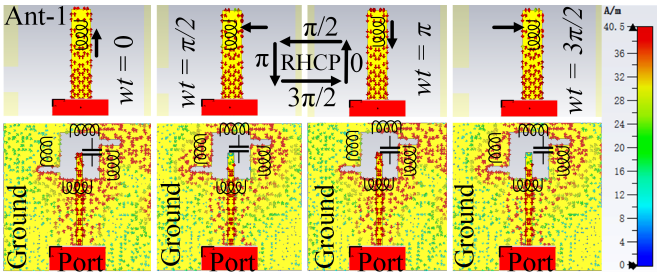


**FIGURE 5.** Surface current vector notation of Ant-1 with ground plane at ($\omega t$ = 0, $\pi$/2, $\pi$ and 3$\pi$/2).

the rectangular slot, the proposed antenna attains a broader IBW of 26.69–28.96 GHz. Moreover, the 3 dB axial ratio bandwidth fully overlaps with the impedance bandwidth, demonstrating effective CP behavior with a gain of 4 dBic, as illustrated in Fig. 3 (a) and (b). As shown in 4, when several antenna elements are integrated on a single substrate with a shared ground plane, the surface waves become the dominant coupling mechanism without (w/o) isolating structures. To address this issue, a "+"-shaped slot is incorporated into the ground plane, effectively suppressing the dominant surface wave between adjacent antenna elements. This enhancement improves electrical isolation without reducing their physical spacing. The slotted ground plane reduces the surface wave propagation, resulting in lower mutual coupling, as shown in Fig. 4(a).

According to circular polarization theory, the CP is achieved when the magnitude ratio satisfies $|E_\theta/E_\varphi| = 1$ (0 dB) and the phase difference between the orthogonal components ($\angle E_\varphi - \angle E_\theta$) is $\pm 90°$. Fig. 4(b) presents the magnitude and phase response of the antenna, showing an amplitude ratio close to unity and a phase difference near $-90°$ across the operating frequency band. The negative phase difference indicates that Ant-1 shows RHCP. These findings are further supported by the observed surface current rotation illustrated in Fig. 5. Fig. 6(a) shows the simulated S-parameters result of the MIMO antenna without and with the incorporation of the "+"-shaped slot. The isolation in MIMO systems is a key performance metric that quantifies the level of coupling between antenna elements. The results show that the quad-port antenna w/o the"+"-shaped slot achieves a 10 dB impedance bandwidth of 25.5 to 29 GHz. However, the S-parameters between element-1 and element-4 (i.e., $|S_{12/21}|$, $|S_{31/13}|$, $|S_{41/14}|$, $|S_{23/32}|$, $|S_{42/24}|$, and $|S_{43/34}|$) ranges only from $-18$ to $-27$ dB across the operating band. The low isolation indicates significant mutual coupling and high correlation among antenna ports, potentially affecting the overall performance and radiation characteristics of the MIMO antenna. One effective method for reducing mutual coupling between antenna elements is to

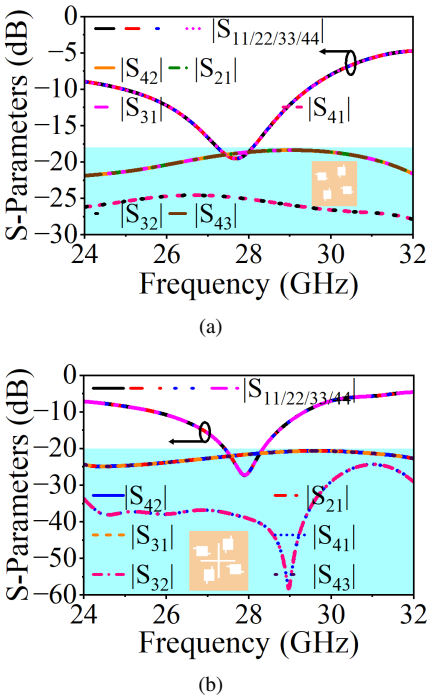


**FIGURE 6.** **Simulated results of S-parameters. (a) Without "+"-shaped slot. (b) With "+"-shaped slot.**

increase the distance between them. However, this approach can lead to an undesirable increase in the overall size of the antenna. To overcome this limitation, it is crucial to design a compact isolating structure that enhances isolation w/o expanding the antenna's size. In this paper, we propose a"+"-shaped slot etched into the ground plane, which effectively reduces correlation among the antenna elements. The MIMO antenna with the "+"-slot exhibits an impedance bandwidth from 26.69 GHz to 28.98 GHz, with an isolation level of at least $\leq -20$ dB throughout this range, as shown in Fig. 6(b).

## III. SRR-Reflector Based MIMO Antenna

The performance of the MIMO antenna can be enhanced in terms of gain and isolation by using a reflector based on a split-ring resonator. Fig. 7(a) shows the SRR unit cell with an equivalent circuit. The dimensions of the SRR unit cell are 7×7 mm $^2$. The equivalent circuit consists of an inductance of $L_1$ = 0.294 nH and a equivalent capacitor of $C_{eq}$ = 0.11 pF [35]. The CST software simulates the SRR reflector using unit cell boundary conditions in the $x$-and-$y$ directions, with Floquet ports for excitation in the $\pm z$-direction. The Keysight advanced design system (ADS) simulates the equivalent circuit model of the proposed SRR. The S-parameters from the CST software and their equivalent circuit are presented in Fig. 7(b). The deepest level of the $|S_{21}|$ is $\leq -$ 65 dB at 28 GHz, while the SRR exhibits bandstop behavior with $|S_{21}| \leq -$ 10 dB from 27.5 GHz to 28.5 GHz. The $|S_{11}|$ value is high in the band stop region shown in Fig. 7(a). In this case, the SRR reflects incoming

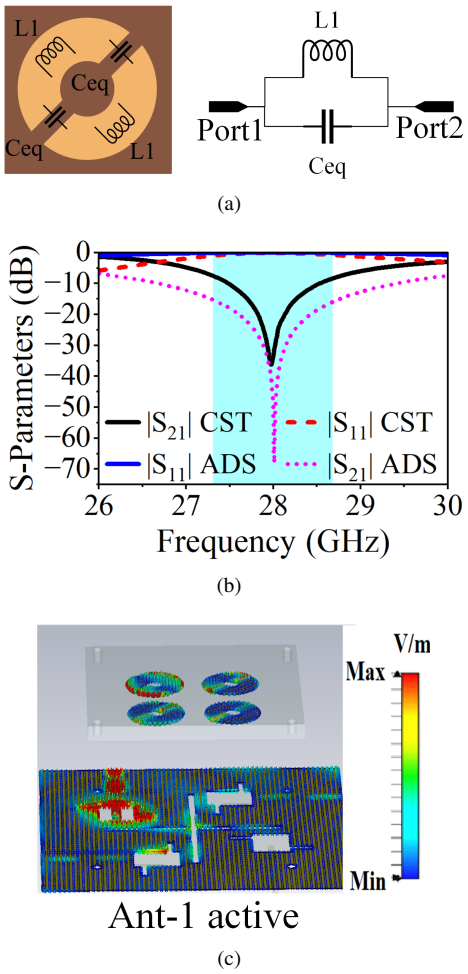


**FIGURE 7.** **(a) SRR unit cell with equivalent circuit model. (b) S-parameter of ECM. (c) Surface-based electric field of Active Ant-1.**

electromagnetic waves at the operating frequency, acting as a reflector. Fig. 7(b) compares the S-parameters from circuit simulators and CST, demonstrating good agreement. Fig. 7(c) illustrates the surface-based electric field of active Ant-1 with SRR-reflecttor at 28 GHz. As can be observed, the "+"-shaped slot blocked the propagated field to deliver another ports. A notable electric field of the Ant-1 is reflected by the SRR-reflector. Fig. 8(a) shows the S-parameters and the port isolation obtained using a reflector. With a reflector, the port isolation is $\leq$ -22 dB throughout the frequency range, and the S-parameter values increase to -35 dB at 28 GHz, as shown in Fig. 8(a). Furthermore, Fig. 8(b) shows the axial ratio and gain with and w/o reflector. Adding a reflector significantly improves the gain from 5 dBic to 6 dBic, resulting in an overall enhancement gain of 1 dBic throughout the entire frequency range and also positively influences the axial ratio within the frequency range of 26.56–28.96 GHz.

## IV. Equivalent Circuit Model

The equivalent circuit model provides a detailed understanding of an antenna's behavior by presenting its operation

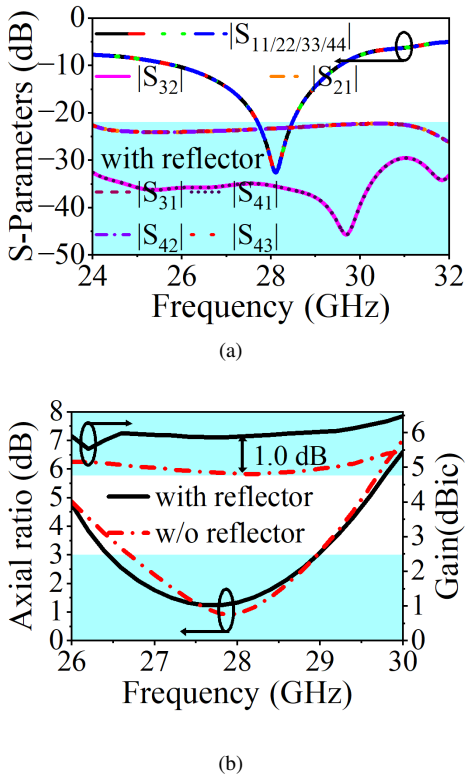


**FIGURE 8.** **Simulated results of MIMO antenna with reflector. (a) S-parameters. (b) Axial ratio with gain (dBic).**

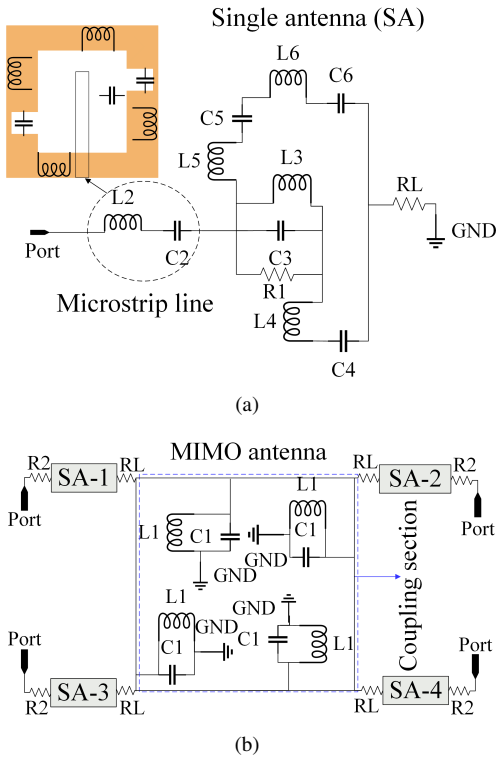


**FIGURE 9.** **(a) Equivalent circuit model of the single antenna (SA). (b) Comparison S-parameters of CST and ADS.**

in terms of lumped circuit elements. The determination of the equivalent circuit for the proposed antenna relies on key parameters such as the feeding line, shape, and number of SRRs. The lumped circuit model is an alternative representation of the equivalent circuit for a conventional planar antenna, which consists of capacitance (C), inductance (L), and resistance (R). The equivalent circuit of a single antenna is modeled and simulated using ADS software, as shown in Fig. 9(a). Four unit cells of the SRR are positioned at a specific height above the quad-port MIMO antenna to reduce mutual coupling. In terms of circuit design, a 2×2 array of SRR is placed centrally and connected in parallel (L, C), as shown in Fig. 9(b). The real and imaginary values helpful in computing the lumped elements calculations are exported from CST. The design consists of four identical elements. Thus, an equivalent circuit of a single-element antenna is sufficient to explain the behavior of the MIMO design. The inductance ($L_0$) and capacitance ($C_0$) of the transmission line at resonance frequency are determined as follows [34]:

$$L_0 = 100h\left(4\sqrt{\frac{W_f}{h}} - 4.21\right) \tag{15}$$

$$C_0 = W_f\left[(9.5\varepsilon_r + 1.25)\frac{W_f}{h} + 5.2\varepsilon_r + 7\right] \tag{16}$$

The remaining lumped elements are calculated using (17) and (18).

$$L = \frac{img\,(Z_{11})}{2\pi f} \tag{17}$$

$$C = \left[(2\pi f)^2 L\right]^{-1} \tag{18}$$

where $W_f$ is the width of feedline and $Z_{11}$ is the port impedance. Now, to determine the port impedance at a specific resonance frequency, first convert the $S_{11}$ parameter into input impedance as follows [34]:

$$Z_{in} = Z_0\frac{(1+S_{11})}{(1-S_{11})} \tag{19}$$

The equation (19) can be presented in a different manner for a better comprehension.

$$Z_{in} = Z_0\frac{[Z_L + jZ_0 tan(\beta l)]}{[Z_0 + jZ_L tan(\beta l)]} \tag{20}$$

where $\beta$ is the propagation constant and $l$ is the feed line length.

In the subsequent step, the input impedance is calculated by combining real and imaginary values.

$$Z_{in} = R_{in} + jX_{in} \tag{21}$$

where $jX_{in}$ is the reactance and $R_{in}$ is the radiation resistance of the resonance frequency.

If $jX_{in}$ value is positive, the reactance is inductive, expressed as

$$X_{in} = \omega L \Rightarrow L = \frac{X_{in}}{\omega} \tag{22}$$

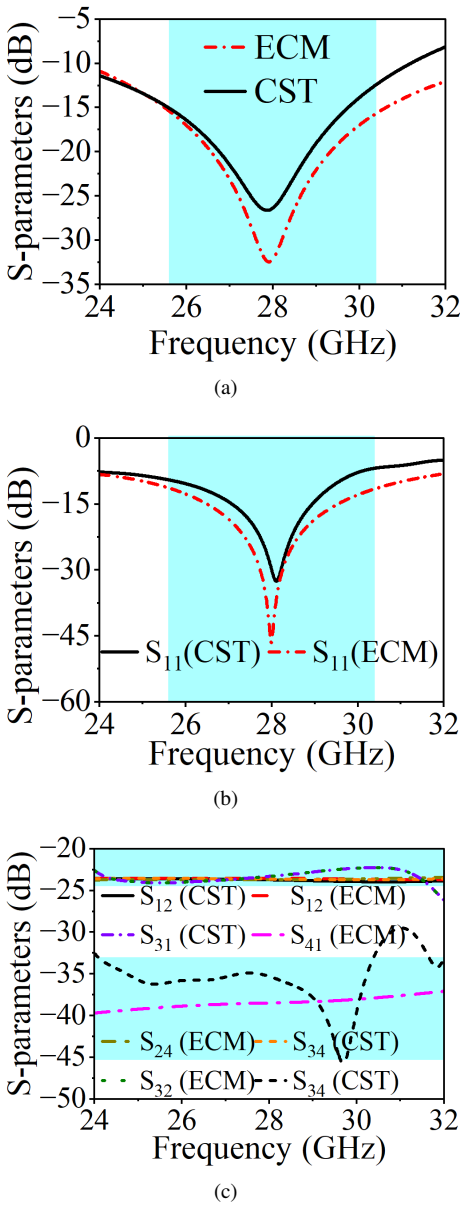


**FIGURE 10.** **(a) Equivalent circuit model of MIMO antenna. (b) Comparison S-parametrs of CST and ADS. (c) S-parameters (Isolation).**

If the value of $jX_{in}$ is negative, the reactance is considered capacitive, which can be calculated using the following formula

$$X_{in} = -\frac{1}{\omega C} \Rightarrow C = -\frac{1}{\omega X_{in}} \tag{23}$$

Finally, the resonant frequency for each branch can be calculated as follows

$$f_r = \frac{1}{2\pi\sqrt{LC}} \tag{24}$$

The four parallel circuits are arranged based on design orientation and mutual coupling after calculating the values of the single-element antenna RLC. The Advanced Design System simulation tool is utilized to validate the S-parameters from CST after calculating all circuit elements. Table 2 lists the optimized RLC values for the single element and the SRR circuit. The S-parameters of single and MIMO antennas show good agreement between the simulated and calculated circuit models, as depicted in Fig. 10(a), (b) and (c). Fig. 10 indicates that the S-parameters from CST and ADS are in good agreement.

**TABLE 2.** **Optimized RLC values of the single and MIMO antenna equivalent circuit model**

| Parameter | Value (mm) | Parameter | Value (mm) | Parameter | Value (mm) |
|---|---|---|---|---|---|
| $L_2$ | 0.254 nH | $C_2$ | 0.108 pF | $L_3$ | 0.294 nH |
| $L_4$ | 0.294 nH | $L_5$ | 0.294 nH | $L_6$ | 0.294 nH |
| $C_3$ | 0.140 pF | $C_4$ | 0.140 pF | $C_5$ | 0.140 pF |
| $C_6$ | 0.140 pF | $R_1$ | 52.8 Ω | $RL$ | 50 Ω |
| $L_1$ | 0.754 nH | $R_2$ | 25.11 Ω | $C_1$ | 0.035 pF |

## V. Experimental Results

Fig. 11 illustrates the fabrication process of the four-port MIMO antenna and the SRR reflector implemented on Rogers RO4003C and RT5880 substrates, with thicknesses of 0.305 mm and 0.508 mm, respectively. The fabricated prototype features: a front view of the microstrip feed line in Fig. 11(a), a back view of the slotted ground in Fig. 11(b), the SRR reflector in Fig. 11(c), and the SRR-based MIMO antenna with a 50 Ω load connector in Fig. 11(d). Fig. 11(e) shows the experimental setup inside an anechoic chamber, using a reference antenna and a vector network analyzer (VNA-ZVA 40). To validate the simulated results, we conducted measurements of the proposed MIMO antenna. Fig. 12 compares the simulated and measured S-parameters, axial ratio, gain (dBic), and radiation efficiency (%). Fig. 12(a) demonstrates a strong agreement between the simulated and measured S-parameters. Fig. 12(b) shows that both simulated and measured S-parameters (isolation) remain below −22 dB across the operating frequency range. Measurements are performed at the boresight direction ($\theta$ = 0°, $\varphi$ = 0°) reveal a 3 dB axial ratio bandwidth of 8.6% (26.56–28.96 GHz) from simulation and 10.01% (26.56–29.36 GHz) from measurement, with peak gain of 6.0 dBic within the same frequency band, as illustrated in Fig. 12(c). Especially, the measured 3 dB axial ratio bandwidth corresponds closely with the simulated 10 dB impedance bandwidth, indicating no polarization mismatch. The radiation efficiency, depicted in Fig. 12(d), exceeds 94% for both simulated and measured data across the entire frequency range. Fig. 13 shows the simulated and measured 2D radiation patterns of the active Ant-1 element at 28 GHz, showing right-hand circular polarization and left-hand circular polarization at $\varphi$ = 0° and 90°. The results clearly indicate that RHCP exhibits a 3 dB wider beamwidth than LHCP. Additionally, the simulated and measured patterns are in good agreement.

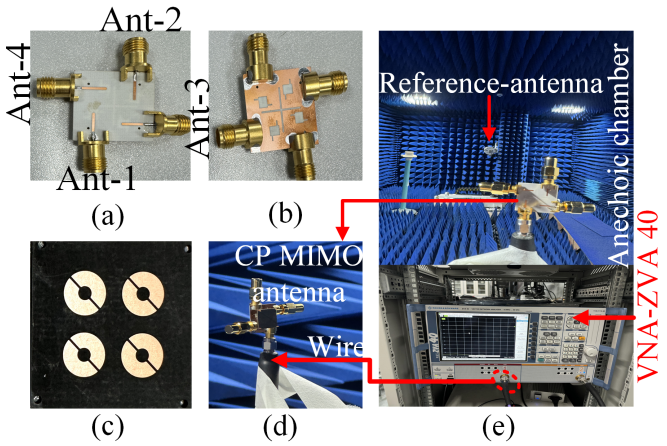


**FIGURE 11.** **Fabricated MIMO antenna. (a) Front view. (b) Back view. (c) SRR-reflector. (d) MIMO antenna with SRR-reflector. (e) Measurements setup.**

## VI. Diversity Performances

Analyzing the diversity parameters [30], [31] in MIMO antennas improve the efficiency, reliability, and performance metrics such as envelope correlation coefficient, diversity gain, mean effective gain, and channel capacity loss. This analysis helps assess the independence of antenna elements and plays a crucial role in multi-path performance, impacting signal propagation paths and reducing correlation factors.

### *A. Envelope Correlation Coefficient*

The envelope correlation coefficient is a crucial factor in assessing the performance of MIMO antennas, as it indicates the independence of antenna elements. A zero ECC is preferred, but systems below 0.5 are acceptable. The ECC should be less than 0.1 for optimal performance, as a lower correlation value indicates better performance. This paper uses the far-field radiation patterns to calculate the ECC for a multi-antenna model in the far field [30].

$$\rho_{porti,portj} = \frac{\frac{1}{2Z_0}\int\int_{\Omega} E_{porti}.E^*_{portj}d\Omega}{\sqrt{P_{rad,porti}}\sqrt{P_{rad,portj}}} \tag{25}$$

where $\Omega$ represents the solid angle. The far-field pattern of the antenna is denoted by $E_{porti}$ when port $i$ is activated, and $E_{portj}$ when port $j$ is excited. The proposed quad-port circularly polarized MIMO antenna exhibits acceptable envelope correlation coefficients across operating frequency bands, as depicted in Fig. 14(a). The simulated and measured ECC values between Ant-1 and Ant-4 (ECC-14) and between Ant-2 and Ant-3 (ECC-23) are depicted in Fig. 14(a). The ECC-14 and ECC-23 exhibit excellent diversity performance, with their values remaining below 0.002 throughout the entire operating frequency band.

### *B. Diversity Gain*

Diversity gain is a crucial parameter in MIMO antenna systems, indicating the influence of the diversity scheme on

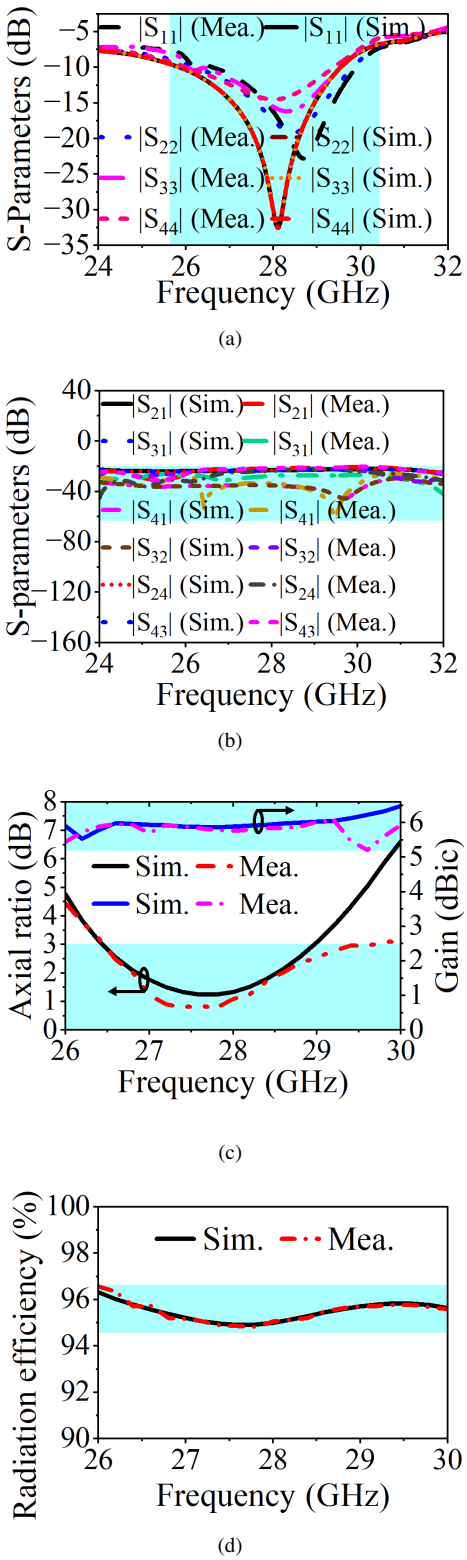


**FIGURE 12.** **Simulated and measured results. (a), (b) S-parameters. (c) Axial ratio with gain (dBic). (d) Radiation efficiency (%).**

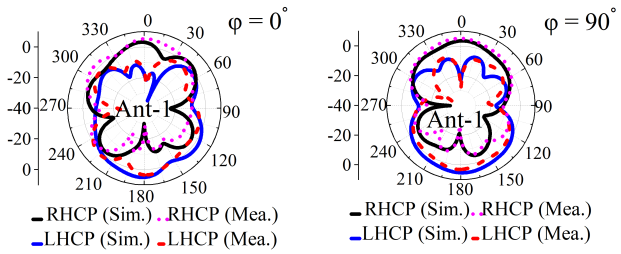


**FIGURE 13.** 2D radiation patterns (RHCP and LHCP) of active Ant-1 at 28 GHz: (a) $\varphi$ = 0° and (b) $\varphi$ = 90°.

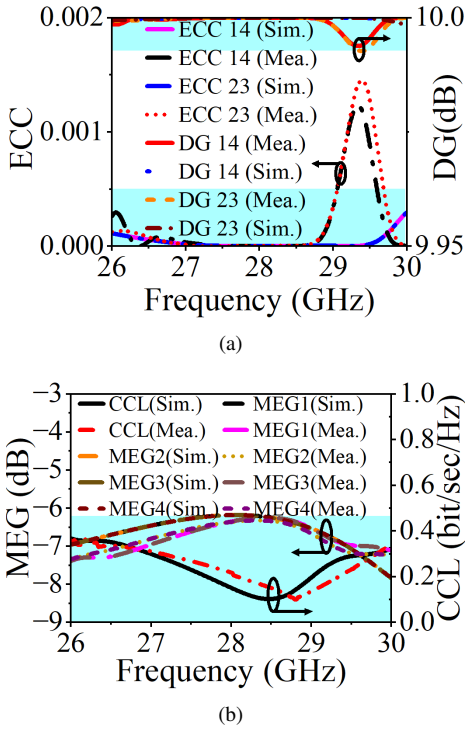


**FIGURE 14.** Simulated and measured results: (a) ECC with DG (dB) and (b) MEG (dB) with CCL (bits/sec/Hz).

transmitted power, calculated using the correlation matrix $\alpha$ [30].

$$DG = \frac{tr\left(\alpha^2\right)}{||\alpha||_{Fr}} \tag{26}$$

The matrix trace $(tr)$ and Frobenius norm $||X\alpha||_{Fr}$ are crucial concepts in matrix analysis. The Frobenius norm is defined as $||\alpha||_{Fr} := \sum_{m,n} |\rho_{mn}|^2$. where $\rho_{mn}$ denotes the elements of the matrix $\alpha$. The matrix trace is the sum of the diagonal elements of the matrix $\alpha^2$. A MIMO antenna typically has a directivity gain between 0 and 1 in magnitude or 0 and 10 dB. Fig. 14(a) shows the variation in the DG of the proposed quad-port CP MIMO antenna, both simulated and measured across the overall frequency range. The MIMO antenna exhibits a DG-14 and DG-23 that surpass 9.99 dB across the entire frequency band, which aligns with the measured results.

### C. Mean Effective Gain

Mean effective gain is a measure of an antenna's efficiency in receiving or transmitting signals, with higher MEG values indicating better performance. MEG values typically fall within a specific range: $-3 \leq$ MEG (dB) $\leq -12$. The mean effective gain for port $i$ can be calculated using (27) [31].

$$MEG_i = 0.5\eta_i, rad = 0.5\left[1 - \sum_{j=1}^{M} |S_{i,j}|^2\right] \tag{27}$$

where $M$ represents the total count of antennas, '$i$' indicates a specific active antenna, and $\eta_i, rad$ denotes the efficiency of the antenna. The simulated quad-port MIMO antenna has a MEG value below the recommended threshold, as shown in Fig. 14(b), which agrees with the measured result.

### D. Channel Capacity Loss

Channel capacity loss is a crucial metric in diversity analysis, indicating the optimal transmission of electromagnetic signals for maximum data rate and minimal distortion. The CCL values in free space are within a limit of $< 0.5$ bits/sec/Hz, and can be calculated using (28)–(31) [31].

$$CCL = -\log_2 det\left(\Psi_{ant}\right) \tag{28}$$

where $\Psi_{ant}$ is the correlation matrix of the antenna and it is given by

$$\Psi_{ant} = \begin{bmatrix} \rho_{11} & \rho_{12} & \rho_{13} & \rho_{14} \\ \rho_{21} & \rho_{22} & \rho_{23} & \rho_{24} \\ \rho_{31} & \rho_{32} & \rho_{33} & \rho_{34} \\ \rho_{41} & \rho_{42} & \rho_{43} & \rho_{44} \end{bmatrix} \tag{29}$$

where

$$\rho_{ii} = 1 - \left|\sum_{n=1}^{n=4} S_{in}^* S_{ni}\right|, \text{for } i,\ j = 1,\ 2,\ 3 \text{ or } 4 \tag{30}$$

and

$$\rho_{ij} = -\left|\sum_{n=1}^{n=4} S_{in}^* S_{nj}\right|, \text{for } i,\ j = 1,\ 2,\ 3 \text{ or } 4 \tag{31}$$

Also, Fig. 14(b) illustrates that the CCL remains below 0.25 bits/sec/Hz across the entire frequency range, further demonstrating robust system performance. Fig. 14(b) demonstrates that the measured and simulated CCL values for the quad-port CP MIMO antenna meet the acceptable limits.

## VII. Comparison

Table 3 provides a comparative analysis of related parameters between the proposed antenna and previous works. Ikram et al. [19] reported on a tapered slot MIMO antenna design capable of dual-band operation in the microwave and mmWave ranges. Lai et al. [29] proposed a ME-dipole antenna using parasitic stubs in the mmWave frequency bands. However, these designs have wide impedance bandwidths and high gain, but large element spacings, low isolation, and low radiation efficiency, primarily featuring linearly polarized radiation without diversity performance. Sofi et

**TABLE 3. Comparison of the proposed MIMO antenna with previous works**

| Reference | [19] | [29] | [30] | [31] | **This Work** |
|---|---|---|---|---|---|
| Year | 2019 | 2024 | 2022 | 2023 | 2025 |
| Size ($mm^3$) | 104.0×104.0 ×0.51 | 42×18 ×1.829 | 23.85×44.90 ×1.52 | 22.5×36.0 ×0.508 | **20.0×20.0 ×0.813 (w/o air)** |
| Number of ports | 4 (high freq.) | 8 | 2 | 2 | **4** |
| Frquency (GHz) | 23–30 | 25.8–35.3 | 29.25–30.35 | 25.84–27.35 | **25.56–28.96** |
| Axial ratio (%) | – | – | 3.69 | 5.6 | **8.60** |
| Element spacing | $0.44\lambda_0$ | $0.44\lambda_0$ | – | $0.61\lambda_0$ | **$0.42\lambda_0$** |
| Polarization | LP | LP | CP | CP | **CP** |
| Gain (dBic) | 11.0 | 6.0 | 4.77 | 6.1 | **6.0** |
| Isolation (dB) | $\geq$ 16 | $\geq$ 17 | $\geq$ 20 | $\geq$ 20 | $\geq$ **22** |
| ECC/ DG (dB) | $\leq$ 0.0001 / – | $\leq$ 0.009 / – | – / $\geq$ 9.99 | $\leq$ 0.003 / $\geq$9.99 | $\leq$ **0.002/** $\geq$ **9.99** |
| MEG (dB)/ CCL (bps/Hz) | – / – | – / – | – / $\leq$ 0.25 | $\leq -$ 6.0 / $\leq$ 0.26 | $\leq -$ **6.0/** $\leq$ **0.25** |
| Radiation efficiency | $\geq$85 | $\geq$95 | $\geq$ 97 | $\geq$ 80 | $\geq$ **94** |
| Size ($\lambda_0^3$) | 9.71×9.71 ×0.047 | 4.2×1.68 ×0.170 | 1.55×2.92 ×0.099 | 2.9×1.8 ×0.04 | **1.87×1.87** × **0.076** |

al. [30] presented a CP MIMO antenna intended for K-/Ka-band satellite applications, while Tiwari et al. [31] detailed a semi-flexible diversified CP wearable antenna for 5G mmWave applications.However, both designs in [30] and [31] exhibit small impedance and axial ratio bandwidths, low gain, and low isolation in mmWave frequency ranges. In contrast, the proposed work presents additional advantages, such as wider impedance bandwidth, axial ratio bandwidth, small element spacings, compact size, and higher isolation. Moreover, the proposed four-port MIMO antenna obtains low ECC and enhanced diversity gain. Hence, the proposed design represents the miniaturized quad-port CP MIMO slot antenna that simultaneously achieves a compact size, wide CP bandwidth, and high radiation efficiency. By integrating a "+"-shaped defected ground structure and an SRR-based reflector, the antenna offers enhanced isolation and gain without increasing footprint. These features make it highly suitable for 5G mmWave communication, Internet of Things (IoT) devices, and next-generation smart wireless systems, where compactness, efficiency, and reliable polarization diversity are essential.

## VIII. Conclusion

A miniaturized quad-port circularly polarized MIMO slot antenna has been investigated, demonstrating high isolation and enhanced diversity performance. The antenna uses four identical rectangular notched slots, each fed by a 50 Ω microstrip line, with an incorporated "+"-shaped slot in the ground to achieve isolation less than −20 dB. A 2×2 array of SRR reflectors is positioned above the antenna to improve gain by approximately 1 dBic and to maintain isolation better than −22 dB. The simulated and measured 10 dB impedance bandwidth and 3 dB axial ratio bandwidth overlap, demonstrating excellent impedance matching and circular polarization performance. The radiation patterns confirm polarization diversity, with a peak gain of 6.0 dBic and radiation efficiency exceeding 94% across the operating frequency range. In addition, diversity metrics such as ECC, DG, MEG, and CCL further confirm the superior performance of the MIMO antenna. Therefore, the proposed CP MIMO antenna is well-suited for mmWave applications.

## REFERENCES


[1] J. G. Andrews et al., "What Will 5G Be?," *IEEE J. Sel. Areas Commun.*, vol. 32, no. 6, pp. 10651082, Jun. 2014.

[2] J. Zhang, X. Yu, and K. B. Letaief, "Hybrid beamforming for 5G and beyond millimeter-wave systems: A holistic view," *IEEE Open J. Commun. Soc.*, vol. 1, pp. 77–91, 2020.

[3] F. A. Dicandia, S. Genovesi and A. Monorchio, "Analysis of the Performance Enhancement of MIMO Systems Employing Circular Polarization," *IEEE Trans. Antennas and Propag.*, vol. 65, no. 9, pp. 4824–4835, Sept. 2017.

[4] U. Ullah, M. Al-Hasan, S. Koziel, and I. B. Mabrouk, "Series-slot-fed circularly polarized multiple-inputmultiple-output antenna array enabling circular polarization diversity for 5G 28 GHz indoor applications," *IET Commun.*, vol. 69, no. 9, pp. 5607–5616, Sep. 2021.

[5] N. Hussain, K. Aljaloud, K., R. Hussain, et al., "Dual-sense slot-based CP MIMO antenna with polarization bandwidth reconfigurability," *Sci. Rep.*, vol. 13, p. 16132, Sep. 2023.

[6] R. Wang, M. Ikram, Y. Yu, H. Zhang and A. Shamim, "Dual-Band Circularly Polarized Shared-Aperture Vivaldi MIMO Antenna With Linear-to-Circular Polarizer for 5G and 6G Communication," *IEEE Trans. Antennas and Propag.*, vol. 73, no. 7, pp. 4300–4310, Jul. 2025.

[7] Y. Dou, Z. Chen, J. Bai, Q. Cai, and G. Liu, "Two-port CPW-fed dual band MIMO antenna for IEEE802.11a/b/g applications," *Int. J. antennas Propag.*, vol. 2021, 2021, Art. no. 5572887.

[8] A. G. Alharbi, J. Kulkarni, A. Desai, C. Y. D. Sim, and A. Poddar, "A multi-slot two-antenna MIMO with high isolation for sub-6 GHz 5G/IEEE802.11ac/ax/C-band/X-band wireless and satellite applications," *Electronics*, vol. 11, no. 3, Feb. 2022, Art. no. 473.

[9] M. H. Reddy, D. Sheela, and A. Swaminath, "A four port circularly polarized printed multiple-input multiple-output antenna with enhanced isolation," *Int. J. Commun. Syst.*, vol. 35, no. 4, Mar. 2022, Art. no. e5061.

[10] Z. Ma, j. Chen, and C. Li, et al., "A monopole broadband circularly polarized antenna with coupled disc and folded microstrip stub lines," *J. Wireless Com. Network*, Art. no. 30. Mar. 2023.

[11] W. Li, et al. "A Wideband Differentially Fed Circularly Polarized Slotted Patch Antenna with a Large Beamwidth," *J. Electromagn. Eng. Sci* , vol. 23, no. 6, pp. 512–520, Nov. 2023.

[12] D. Wu, J. Liang and L. Ge, "A Wideband Dual-Circularly Polarized Series-Fed Corner-Truncated Patch Array Using Coplanar Proximity Coupling," *IEEE Trans. Antennas and Propag.*, vol. 72, no. 4, pp. 3292–3301, Apr. 2024.

[13] S. M. Mikki and Y. M. M. Antar, "On cross correlation in antenna arrays with applications to spatial diversity and MIMO systems," *IEEE Trans. Antennas and Propag.*, vol. 63, no. 4, pp. 1798–1810, Apr. 2015.

[14] Y. Banday, G. M. Rather and G. R. Begh "Effect of atmospheric absorption on millimetre wave frequencies for 5G cellular networks," *IET Commun.*, vol. 13, no. 3, pp. 265–270, Feb. 2019.

[15] M. H. Reddy, D. Sheela, and A. Swaminath, "A four port circularly polarized printed multiple-input-multiple-output antenna with enhanced isolation," *Int. J. Commun. Syst.*, vol. 35, no. 4, Mar. 2022, Art. no. e5061.

[16] H. Zahra, W. A. Awan, W. A. E. Ali, N. Hussain, S. M. Abbas, and S. Mukhopadhyay, "A 28 GHz broadband helical inspired end-fire antenna and its MIMO configuration for 5G pattern diversity applications," *Electronics*, vol. 10, no. 4, p. 405, Feb. 2021.

[17] I. Khan et al., "Dual-Technique MIMO Antenna Design for IoT Millimeter-Wave Circular Polarization," *IEEE Antennas Wireless Propag. Lett.*, vol. 24, no. 8, pp. 2158–2162, Aug. 2025.

[18] F. Lin, Y. Qi, J. Fan and Y. -C. Jiao, "0.7–20-GHz Dual-Polarized Bilateral Tapered Slot Antenna for EMC Measurements," *IEEE Trans. Electromagn. Compat.*, vol. 56, no. 6, pp. 1271–1275, Dec. 2014.

[19] M. Ikram, N. Nguyen-Trong and A. Abbosh, "Multiband MIMO Microwave and Millimeter Antenna System Employing Dual-Function Tapered Slot Structure," *IEEE Trans. Antennas and Propag.*, vol. 67, no. 8, pp. 5705–5710, Aug. 2019.

[20] Y. Xiao et al., "A Planar Low-Profile Meander Antenna Design for Wireless Terminal Achieving Low RF Interference and High Isolation

in Multi-Antenna Systems," *IEEE Trans. Electromagn. Compat.*, vol. 64, no. 3, pp. 674–682, Jun. 2022.
[21] G. Santra and P. N. Patel, "Horizontally Polarized Omnidirectional Antenna Using Slotted Rectangular Patch and Defected Ground Structure," *IEEE Antennas Wireless Propag. Lett.*, vol. 22, no. 4, pp. 704–708, Apr. 2023.
[22] H. Jiang et al., "A Compact Triple-Band Antenna With a Notched Ultra-Wideband and Its MIMO Array," *IEEE Trans. Antennas and Propag.*, vol. 66, no. 12, pp. 7021-7031, Dec. 2018.
[23] I. Khan, K. Zhang, L. Ali and Q. Wu, " A Compact FSS-Based Four-Port MIMO Antenna for Low Mutual Coupling," *IEEE Antennas Wireless Propag. Lett.*, vol. 22, no. 12, pp. 2836–2840, Dec. 2023.
[24] L. Wang et al., "Compact UWB MIMO Antenna With High Isolation Using Fence-Type Decoupling Structure," *IEEE Antennas Wireless Propag. Lett.*, vol. 18, no. 8, pp. 1641–1645, Aug. 2019.
[25] S. Li and Q. -X. Chu, "Broadband Mutual Coupling Reduction of Multiple Electrical-Current Nulls for Quad-Port Shared-Radiator Slot Antenna Using Characteristic Mode Analysis," *IEEE Antennas Wireless Propag. Lett.*, vol. 23, no. 1, pp. 409–413, Jan. 2024.
[26] N. Alaa, R. A. Elsayed and A. E. Farahat et al., "Q-Band MIMO Antennas with Circular Polarization for Spatial and Polarization Diversity," *J. Infr. Milli. Terahz. Waves*, vol. 45, pp. 393–432, Jun. 2024.
[27] I. Khan, K. Zhang, L. Ali and Q. Wu, "Enhanced Quad-Port MIMO Antenna Isolation With Metamaterial Superstrate," *IEEE Antennas Wireless Propag. Lett.*, vol. 23, no. 1, pp. 439–443, Jan. 2024.
[28] M. J. Al-Hasan, T. A. Denidni and A. R. Sebak, "Millimeter-Wave Compact EBG Structure for Mutual Coupling Reduction Applications," *IEEE Trans. Antennas Propag.*, vol. 63, no. 2, pp. 823-828, Feb. 2015.
[29] Q. X. Lai, Z. L. Hu and Y. M. Pan, "A Simple Decoupling Method for Wideband Millimeter-Wave MIMO Magnetoelectric Dipole Antenna Array Using Parasitic Stubs," *IEEE Trans. Antennas Propag.*, vol. 72, no. 10, pp. 7470–7479, Oct. 2024.
[30] M. A. Sofi, K. Saurav and S. K. Koul, "Four-Port Orthogonal Circularly Polarized Dual-Band MIMO Antenna With Polarization and Spatial Diversity Using a Dual-Band Linear-to-Circular Polarization Converter," *IEEE Trans. Antennas Propag.*, vol. 70, no. 9, pp. 8554–8559, Sep, 2022.
[31] R. N. Tiwari, V. Kaim, P. Singh, T. Khan and B. K. Kanaujia, "Semi-Flexible Diversified Circularly Polarized Millimeter-Wave MIMO Antenna for Wearable Biotechnologies," *IEEE Trans. Antenna Propag.*, vol. 71, no. 5, pp. 3968–3981, May, 2023.
[32] F. Merzaki et al., "A Compact Double-Sided FSS Absorbing Wall for Decoupling 5G Antenna Arrays," *IEEE Trans. Electromagn. Compat.*, vol. 64, no. 2, pp. 303–314, Apr. 2022.
[33] G. Ramyasree and N. Suman, "Dual-band 4-port vivaldi MIMO antenna for 5G mmwave applications at 28/39 GHz," *Prog. Electromagn. Res.*, vol. 119, pp. 13–24, May 2023.
[34] S. Khan et al., "Highly Compact Wideband High-Gain Four-Element MIMO Antenna for 5G New Radio IoT," *IEEE Internet Things J.*, vol. 12, no. 12, pp. 22350–22365, Jun. 15, 2025.
[35] F. Bilotti, A. Toscano, and L. Vegni, "Design of spiral and multiple split-ring resonators for the realization of miniaturized metamaterial samples," *IEEE Trans. Antennas Propag.*, vol. 55, no. 8, pp. 2258-2267, Aug. 2007.

**Abdul Majeed** received the Master of Philosophy in Electronics (Electromagnetic and Microwave Engineering) from Quaid.i-Azam University, Islamabad, Pakistan in 2017. In 2018, he started PhD in Electronic Science and Technology at Beijing University of Posts and Telecommunications, Beijing China and in September, 2023, he received a PhD Engineering degree. He has authored or coauthored in more than 17 peer-reviewed journal papers and conferences of international reputation. Currently, he is a post-doctoral fellow at Shenzhen Key Laboratory of Antennas and Propagation, Shenzhen University. His research interests include Optical and transparent metasurfaces meta-antennas, MIMO antenna, electromagnetic wave and propagation, RF/microwave engineering, wireless power transmission, micro/mm-Waves system and devices, surface plasmon resonance, chiral, and bi-isotropic substrate. He also serves as a Regular Reviewer for reputed international journals, including the IEEE, Elsevier, Springer, Optica, and International Journal for Light and Electron Optics.

**Yejun He** (Senior Member, IEEE) received the Ph.D. degree in Information and Communication Engineering from the Huazhong University of Science and Technology (HUST), Wuhan, China, in 2005. From 2005 to 2006, he was a Research Associate with the Department of Electronic and Information Engineering, The Hong Kong Polytechnic University, Hong Kong. From 2006 to 2007, he was a Research Associate with the Department of Electronic Engineering, Faculty of Engineering, The Chinese University of Hong Kong, Hong Kong. In 2012, he joined the Department of Electrical and Computer Engineering, University of Waterloo, Waterloo, ON, Canada, as a Visiting Professor. From 2013 to 2015, he was an Advanced Visiting Scholar (Visiting Professor) with the School of Electrical and Computer Engineering, Georgia Institute of Technology, Atlanta, GA, USA. From 2023 to 2024, he was an Advanced Research Scholar (Visiting Professor) with the Department of Electrical and Computer Engineering, National University of Singapore, Singapore.

Since 2006, he has been a faculty of Shenzhen University, where he is currently a Full Professor with the College of Electronics and Information Engineering, Shenzhen University, Shenzhen, China, the Director of Sino-British Antennas and Propagation Joint Laboratory of Ministry of Science and Technology of the People's Republic of China (MOST), the Director of the Guangdong Engineering Research Center of Base Station Antennas and Propagation, and the Director of the Shenzhen Key Laboratory of Antennas and Propagation. He was selected as an Expert with Special Government Allowance from the State Council in China, and a Leading Talent in the "Guangdong Special Support Program" in 2024. He was promoted to the Shenzhen "Pengcheng Scholar" Distinguished Professor in 2020. He has authored or coauthored more than 350 refereed journal and conference papers and seven books. He holds more than 30 patents. His research interests include wireless communications, antennas, and radio frequency.

Dr. He was also a recipient of the Shenzhen Overseas High-Caliber Personnel Level B (Peacock Plan Award B) and Shenzhen High-Level Professional Talent (Local Leading Talent). He received the Second Prize of Shenzhen Science and Technology Progress Award in 2017, the Three Prize of Guangdong Provincial Science and Technology Progress Award in 2018, the Second Prize of Guangdong Provincial Science and Technology Progress Award in 2023, and the 10th Guangdong Provincial Patent Excellence Award in 2023. He is currently the Chair of IEEE Antennas and Propagation Society-Shenzhen Chapter and obtained the 2022 IEEE APS Outstanding Chapter Award. He has served as a Technical Program Committee Member or a Session Chair for various conferences, including the IEEE Global Telecommunications Conference (GLOBECOM), the IEEE International Conference on Communications (ICC), the IEEE Wireless Communication Networking Conference (WCNC), and the IEEE Vehicular Technology Conference (VTC). He served as the TPC Chair for IEEE ComComAp 2021 and the General Chair for IEEE ComComAp 2019. He was selected as a Board Member of the IEEE Wireless and Optical Communications Conference (WOCC). He served as the TPC Co-Chair for WOCC 2023/2022/2019/2015, APCAP 2023, UCMMT 2023, ACES-China2023, NEMO 2020 and so on. He acted as the Publicity Chair of several international conferences such as the IEEE PIMRC 2012. He has served as an Executive Chair of 2024/2025 IEEE International Workshop of Radio Frequency and Antenna Technologies. He is the Principal Investigator for over 40 current or finished research projects, including the National Natural Science Foundation of China, the Science and Technology Program of Guangdong Province, and the Science and Technology Program of Shenzhen City. He has served as a Reviewer for various journals, such as the IEEE Transactions on Vehicular Technology, the IEEE Transactions on Communications, the IEEE Transactions on Industrial Electronics, the IEEE Transactions on Antennas and Propagation, the IEEE Wireless Communications, the IEEE Communications Letters, the International Journal of Communication Systems,and Wireless Personal Communications.

Dr. He is a Fellow of IET, and a Fellow of China Institute of Communications (CIC). He is serving as an Associate Editor for IEEE Transactions on Vehicular Technology, IEEE Transactions on Antennas and Propagation,

IEEE Transactions on Mobile Computing, IEEE Antennas and Wireless Propagation Letters, IEEE Antennas and Propagation Magazine, International Journal of Communication Systems, China Communications, and ZTE Communications.

**Yi Huang**(Fellow, IEEE) received DPhil degree in Communications from the University of Oxford, UK in 1994. He has been conducting research in the areas of wireless communications, applied electromagnetics, radar, and antennas since 1987. His experience includes 3 years spent with NRIET (China) as a Radar Engineer and various periods with the Universities of Birmingham, Oxford, and Essex in the UK as a member of research staff. He worked as a Research Fellow at British Telecom Labs in 1994 and then joined the Department of Electrical Engineering & Electronics, the University of Liverpool, UK as a Faculty in 1995, where he is now a full Professor in Wireless Engineering, the Head of the High Frequency Engineering Group. Dr Huang has published over 500 refereed papers in leading international journals and conference proceedings and authored books on Antennas: from Theory to Practice (John Wiley, 2008, and 2021) and Reverberation Chambers (Wiley 2016, and 2019). He has received over 10 awards (e.g. the IET Premium Award 2022 for Best Paper, EuCAP2023 Best Antenna Paper, the IET Innovation Award 2018, and BAE Systems Chairman's Award 2017) and many research grants from research councils, government agencies, charities, the EU, and industry, acted as a consultant to various companies, and served on a number of national and international technical committees (such as the IET, EPSRC, European COST-IC0603, and COST-IC1102, and EurAAP) and been an Editor, Associate Editor or Guest Editor of four of international journals (including IEEE AWPL 2016-2022). He has been a keynote/invited speaker and organiser of many international conferences and workshops (e.g. EuCAP2018/2024, IEEE iWAT, WiCom, and LAPC). He is at present the Editor-in-Chief of Wireless Engineering and Technology, Associate Editor of IEEE Trans on Antennas and Propagation, the UK/Ireland Delegate to EurAAP (2016-2020, 2022-2024), a Fellow of IEEE, a member of IEEE AP-S New Technology Directions Committee, and a Distinguished Lecturer of IEEE AP-S (2022-2025).